Final Draft
of the original manuscript:

Yi, S.; Bohlen, J.; Heinemann, F.; Letzig, D.**:**
Mechanical anisotropy and deep drawing behaviour of AZ31 and ZE10 magnesium alloy sheets
In: Acta Materialia (2009) Elsevier

DOI: 10.1016/j.actamat.2009.09.038

Mechanical anisotropy and deep drawing behaviour of AZ31 and ZE10 magnesium alloy sheets

Sangbong Yi, Jan Bohlen, Frank Heinemann, Dietmar Letzig

Magnesium Innovation Centre, GKSS Research Centre, Max-Planck-Str., D-21502, Geesthacht, Germany

Abstract

The influence of the initial microstructure on the deep drawability and the associated microstructural evolution in two different magnesium alloy sheets, AZ31 and ZE10, has been examined. Tensile testing at room temperature shows that the AZ31 sheet has high plastic strain ratios, r = 2 ~ 3, which are caused by strong basal-type texture. The ZE10 sheet shows lower r values, r ~ 1, as a result of its weak texture. Deep drawing experiments carried out over the temperature range 100-300 °C revealed that the ZE10 sheet can be successfully deep drawn at lower temperatures than AZ31 sheet. The ZE10 cups show earing despite the weak texture and low normal anisotropy, while earing of the AZ31 cups is negligible. In the ZE10 cups, deformation is accommodated mainly by <a> slips and by compression as well as secondary twinning. The occurrence of dynamic recrystallisation is observed in successfully deep-drawn AZ31 cups.

Keywords: Magnesium alloys; Mechanical properties; Texture; Deep drawing; Dynamic recrystallisation.

Corresponding author:

Sangbong Yi

E-mail) sangbong.yi@gkss.de

Tel) +49-4152-87 1911
Fax) +49-4152-87 1927

1. Introduction

The poor formability of magnesium sheets, especially at room temperature, is one of the main factors hindering industrial application of semi-finished products of this lightest structural metallic material. Traditional wrought alloys, e.g. those based on the Mg-Al-Zn system such as AZ31, have a tendency to develop a strong basal-type texture during the sheet rolling process [1-4]. This basal-type texture, in which most grains have their c-axes in the sheet normal direction (ND), limits sheet formability because it restricts the activity of <a> dislocation slip, especially under loading in the ND. Although strain along the ND can in principle be accommodated by pyramidal <c+a> slip, this deformation system can only be activated at relatively high temperature because of its high critical resolved shear stress (CRSS) at low temperature [5]. In order to improve the formability of magnesium sheets, it is necessary to provide a way of weakening the texture or, more generally, avoiding the strong basal-type texture. In the case of a weak basal-type texture, it is expected that <a> dislocations with a relatively low CRSS will contribute more to accommodating the deformation.

One effective way of altering the strong basal-type texture is to impose a large shear deformation during rolling. For example, sheets produced by asymmetric rolling exhibit a weak texture with basal poles slightly rotated towards the rolling direction (RD) [6-8]. Another approach to controlling texture is to modify the alloy composition. It has been reported recently that weakening of the texture can be achieved by alloying magnesium with yttrium (Y) and rare earth (RE) elements such as cerium (Ce) or neodynium (Nd) [9-11]. Moreover, increased ductility has been observed in sheets having a weaker texture [9, 12, 13].

A number of recent publications have dealt with the optimisation of processing parameters and their effects on the formability of magnesium sheets [14-18], especially during deep drawing, which is an important and popular forming process for the production of flat components [19]. However, the effects of the initial texture and microstructure on sheet formability, which in turn influence the evolution of texture and microstructure during the forming process, are still unclear.

The present study was carried out to contribute to a basic understanding of the influence of the initial texture on the mechanical properties and the formability using two commercial Mg sheets which show distinct textures and comparable grain size, namely AZ31 and ZE10 alloys. The mechanical anisotropy and the earing behaviour during cup drawing were examined with emphasis on the role of texture.

2. Experimental procedures

Rolled sheets of two commercial magnesium alloys, AZ31 (2.8 Al-0.8 Zn-0.2 Mn in wt. %) and ZE10 (1.3 Zn-0.2 Ce-0.1 La), with thickness of 1.3 mm were examined in the present study.

Tensile samples in the RD, at 45° and in the transverse direction (TD) with a gauge length of 50 mm and a width of 12.5 mm were prepared using discharge machining. Tensile tests were conducted using a universal testing machine, Zwick 050, at room temperature with an initial strain rate of $1\times10^{-3}\,s^{-1}$. Two extensometers were employed to measure the strain in the length and width direction simultaneously. The plastic strain ratio, r value, is calculated using the strain values within the uniform elongation, commonly at 20 % of the elongation in cubic materials [20]. However, the present materials show fracture strains lower than 20 %. It was reported recently that uniform elongation is observed up to 10 % in both alloys and that the r value varies very slightly with the tensile elongation [21]. Hence, in the present study, the r value was calculated at 8% engineering strain in the tensile direction as

$$r_8 = \frac{\varepsilon_{w\_8}}{\varepsilon_{t\_8}} = \frac{\varepsilon_{w\_8}}{-(\varepsilon_{l\_8} + \varepsilon_{w\_8})} \quad , \ \varepsilon_l + \varepsilon_t + \varepsilon_w = 0 \text{ during plastic deformation} \qquad (1)$$

where ε_{t_8}, ε_{w_8}, and ε_{l_8} are the plastic strains in the sample thickness *t*, width *w* and length *l* directions at 8 % engineering tensile strain. The results of the tensile tests presented in this study are the average values obtained from at least 3 stress-stain curves for each condition.

Round blanks with diameter of 85 mm were prepared for the deep drawing tests. Deep drawing experiments were conducted using an Erichsen universal sheet testing machine with a drawing ratio, β = blank diameter / punch diameter, of 1.7 at different temperatures, 150, 200, 250 and 300 °C. The blanks were heated to working temperature together with the blank holder in an extra furnace and were mounted in the testing machine after reaching the desired temperature. The punch speed and the blank holder force were kept constant for all test temperatures at 20 mm/min and 5 kN, respectively. The whole blank and the contact area of the punch were coated with boron nitride spray as lubricant. The planar anisotropy of the rolled sheets, which is also visible as strong variation of r values in different sample directions, is recognised to cause so-called ears on the drawn cup, which means a variation of height along the wall of the deep drawn cup. To describe the degree of earing, by convention, the average percentage of earing height (z) is typically calculated as

$$z = \frac{h_0 + h_{90} - h_{45}}{\bar{h}} \times 100 \quad (\%) \qquad (2a)$$

where *h* represents the height at 0°, 45° and 90° from the RD. $\bar{h}$, the average height is calculated as

$$\bar{h} = \frac{h_0 + h_{45} + h_{90}}{3} \qquad (2b)$$

The ears observed in the present study are located mainly at 60° to the RD. Moreover, there are also differences in the height of the ears in each cup itself depending on their location. Thus, in the present work, another definition of Z is preferred

$$Z = \left\{ \left[\sum_{i}^{n} \frac{(h_{i\_\max} - h_{i\_\min})}{0.5(h_{i\_\max} + h_{i\_\min})} \right] / n \right\} \times 100 \quad (\%) \qquad (3)$$

where n is the number of the ears in the drawn cup. This notation is capable of describing earing even if a local asymmetry occurs and takes ears of different orientations into account.

Global texture information on the initial sheets was obtained using X-ray diffraction (Panalytical, 40 kV and 40 mA). The microstructure and the texture of the rolled sheets and the deep drawn cups were investigated using electron backscatter diffraction (EBSD) in a field emission gun scanning electron microscope (Zeiss, Ultra 55, working at 15 kV, equipped with an EDAX/TSL EBSD system with a Hikari detector). Samples for EBSD measurements were taken from longitudinal sections of the initial sheets as well as from the drawn cups along the RD. The samples were prepared by mechanical polishing using alumina powder, followed by electrolytic polishing using a Struers AC2 solution (for 60 s at 16 V and -15 °C).

3. Results and Discussion

3.1. Microstructure and mechanical properties of the rolled sheets

The microstructures of the rolled sheets of AZ31 and ZE10 are shown in Fig. 1 as EBSD inverse pole figure maps in the ND. A small fraction of non-indexed points during the EBSD measurements are marked as black. Both alloys show equiaxed grain structures without twins. Mono-modal grain size distributions are observed in both alloys as shown in Fig. 1(c). The grain size of the AZ31 sheet is more homogeneous than that of the ZE10 sheet. The largest frequency in the grain size is found at 10 μm in the AZ31 sheet and 14 μm in the ZE10 sheet.

Fig. 2 displays recalculated (0001) and $\{10\bar{1}0\}$ pole figures of the two sheets as obtained from XRD measurements. The (0001) pole figure of the ZE10 sheet has a maximum intensity of P_{max} = 2.7 which is much weaker than that of the AZ31 having P_{max} = 13.1. The pole figures of the AZ31 sheet show that most grains have their c-axes in the ND, which corresponds to a so called basal-type texture. The other important feature of the AZ31 sheet

texture is a broader intensity spread of the basal poles from the ND toward the RD than to the TD, Fig. 2 (c). This type of texture has often been referred to as the typical texture of rolled or rather tempered Mg alloy sheets [22-24]. Kaiser et al reported that this type of texture develops during the static recrystallisation of strain hardened AZ31 sheets which show symmetrical splitting of the basal poles towards the RD [24]. Agnew et al have claimed that this symmetrical splitting of the basal poles towards the RD results from the high activation of <c+a> slip during rolling [22, 23]. Another mechanism that promotes this spread of the basal poles is the operation of $\{10\bar{1}1\}$-$\{10\bar{1}2\}$ secondary twinning. A matrix grain, with its c-axis almost parallel to the ND, is deformed firstly by $\{10\bar{1}1\}$ compression twinning and is then re-twinned by $\{10\bar{1}2\}$ tensile twinning [25, 26]. Interestingly, the (0001) pole figure of the ZE10 sheet exhibits an ellipsoidal form of the intensity distribution. The splitting angle of the basal pole from the ND toward the RD is about 25°, which is larger than that in the AZ31 sheet. Furthermore, rotation of the basal poles by about 40° toward the TD is observed, which does not occur in AZ31. This asymmetric distribution of the basal poles around the ND is clearly visible in Fig. 2 (d), which presents the intensity profiles in the (0001) pole figures from the ND to the RD, the TD and 45° direction. This unusual type of texture developed during sheet rolling has been noted by many authors. It has been reported that additions of RE elements to Mg alloys leads to the development of weaker textures during rolling or extrusion, however, a number of different mechanisms for this have been suggested [9, 10, 13, 27-30]. The formation of the more randomised texture in the RE-containing alloys is related mainly to the recrystallisation process, since the rolling texture prior to recrystallisation is similar to that of traditional wrought Mg alloys [30]. Mishra et al [13] and Ball et al [28] suggested that the weaker textures in RE-containing Mg alloys are caused by particle-stimulated nucleation (PSN) and boundary pinning at Mg-RE precipitates. Mackenzie et al [27] deduced that a change in the mobility of high angle boundaries by alloying additions, in the form of a solute drag effect, leads to texture weakening as well as the development of the prominent basal

component rotated toward the TD as also seen in the ZE10 sheet of this study. Nucleation at shear bands formed during the deformation process and a consequent weak texture has been discussed by Stanford & Barnett [29]. All the above mechanisms are viable and have the potential to weaken the resulting textures although it is not yet understood which of these plays the main role during the recrystallisation of Mg-RE alloys.

Stress-strain curves of AZ31 and ZE10 sheets tested in the three selected loading directions (RD, 45° and TD) are shown in Fig. 3. The corresponding mechanical properties are listed in Table 1. Both alloys exhibit in-plane anisotropy in the yield strength and the r value, while the ultimate tensile strength (UTS) is not significantly affected by the sample orientation. The yield strength in the TD of the AZ31 sheet is higher than that measured at 45° and in the RD, while the maximum yield strength of the ZE10 sheet is measured in the RD. In general, the AZ31 sheet shows higher yield strengths and r_8 values in all sample orientations compared to the ZE10 sheet. Moreover, the planar anisotropy, which is the variation of the r_8 values as a function of the tensile loading direction, is also different for the two alloys; the highest r_8 value of the ZE10 sheet is found at 45°, while the r_8 value of the AZ31 sheet tends to increase from the RD to the TD.

This gradual increase in yield strength and r value from the RD to the TD agrees with the results presented by Kaiser et al [24] for rolled AZ31 sheet. This is explained by the broader angular tilt of the basal planes in the RD than in the TD. A larger tilt angle to the RD eases the activation of <a> dislocation slip during loading in this direction compared to the TD. The same explanation holds for the increase of the r value from the RD to the TD. Strain along the thickness direction can be accommodated more easily by basal <a> slip during testing in the RD than in the TD. Because the r value is inversely proportional to the thickness strain, the r value in the RD is smaller than in the TD. In other words, the accommodation of strain in the width of the samples is easier if the basal planes are more tilted to the width direction of the sample, which holds for the test in the TD. Furthermore, the TD sample has prismatic planes

parallel to the width direction, Fig. 2. This orientation is favourable for accommodating width strain ε_w by prismatic <a> slip. For the above reasons, the r value in the RD is lower than that in the TD.

The variation in the yield strength of the ZE10 sheet can also be explained by its texture. Since the pole density of the tilted basal planes and the tilt angle is higher in the TD than in the RD, loading in the TD is advantageous for basal <a> slip. Consequently, the yield strength in the TD is lower than in the RD. In contrast to the r values measured in AZ31, the r values close to 1 in the ZE10 alloy indicate that the cross-sectional contraction occurs isotropically, i.e. the strains in the width (ε_w) and thickness (ε_t) directions are similar. The variation of the r value in different loading directions has a strong relationship with the texture. Fig. 4 shows the relationship between ε_w and ε_l during tensile loading in different planar directions of the AZ31 and ZE10 sheets. During tensile loading in the RD of the AZ31 sheet, a relatively high ε_l is achieved based on the tilted basal planes in the tensile loading direction. During tensile loading in the TD, the sample width direction possesses relative easiness of <a>-dislocation slip which results in a high ε_w in the TD sample compared to the RD and 45° samples, Fig. 4 (a). In contrast to the AZ31 sheet with its high normal anisotropy, the through-thickness deformation in the ZE10 sheet is easy as a result of the weak texture with the high angle of tilt of the basal planes from the ND. The relatively high r value of the 45° sample compared to those of the RD and TD samples of the ZE10 sheet can be explained by the high width strain, Fig. 4 (b). In the case of the RD (or TD) sample, the basal planes tilted towards the TD (or RD) have a low Schmid factor for <a> slip for the width strain component. However, in the case of the 45° sample the basal poles tilted towards the RD as well as the TD are beneficial for strain in the width direction. With the relatively high ε_w in the 45° sample, a high r value is obtained in this direction compared to the RD and TD samples.

3.2. Deep drawing behaviour at different temperatures

The deep drawability of the AZ31 and ZE10 sheets is listed in Table 2. For successful forming, the AZ31 sheet should be heated up to 200 °C, whereas the ZE10 sheet can be drawn at 150 °C. The cups formed at different temperatures are shown in Fig. 5, in which the rolling direction is marked by white arrows. The AZ31 cup drawn at 150 °C shows failure at the corner where a high degree of deformation is applied and strain in the thickness direction (necking) is required. Thus, the probability of failure is high in general. However, the failure of the ZE10 cup occurs at the top part of the wall, which is a typical failure caused by non-optimised process parameters, such as blank holder force and clearance. It is therefore anticipated that the ZE10 sheet could be successfully deep-drawn even at 100 °C, if optimised process parameters are applied.

It is generally expected that high r values favour sheet formability and will lead to higher limiting drawing ratios [19]. For other hexagonal metals, e.g. Ti and Zn, increases in the limiting drawing ratio with the average r values have also been observed [31]. The average plastic strain ratio is typically defined as:

$$\bar{r} = \frac{(r_{RD} + r_{TD} + 2r_{45})}{4} \tag{4}$$

Table 3 compares the results for the two sheets, showing that the $\bar{r}$ value for AZ31 is more than twice as large as that for ZE10 sheet. However, the ZE10 sheet exhibits better drawability in terms of the lower working temperature for successful deep drawing. The results indicate that the relationship between the r values and sheet formability of magnesium alloys should be interpreted in a different way than is usually done for cubic metals. For example, the high r values of the AZ31 sheet can be interpreted as a large mechanical anisotropy and general difficulty of deformation, which result in the lower formability and early fracture.

Fig. 6 shows the degree of earing, Z as defined in Eq. 3, as measured from the successfully drawn cups. In ZE10, four ears are observed, which are located mainly at 60° to the RD with a relatively large deviation of ± 10° in each cup as well as between cups which were drawn at different temperatures. This deviation in the earing positions is likely to be a result of the low texture symmetry of the ZE10 sheet. As seen in Fig. 2, the pole figures of the ZE10 sheet do not show orthorhombic sample symmetry, i.e. the maximal pole densities and their angular positions in each quarter of the (0001) pole figure vary. Notably, the successfully drawn AZ31 cups show almost negligible earing

The earing height of a deep drawn cup is supposed to be dependent on the planar anisotropy [19]. The magnitude of the planar anisotropy is typically defined as Δr,

$$\Delta r = \frac{r_{RD} + r_{TD} - 2r_{45}}{2} \tag{5}$$

The Δr values calculated using the above equation are listed in Table 3. In order to relate the planar anisotropy to the earing behaviour, normalisation of Δr by the average value $\bar{r}$ is required, e.g. $2\Delta r / \bar{r}$ as suggested by Wilson et al [32]. The normalised values are also given in Table 3. The higher absolute value of $2\Delta r / \bar{r}$ for ZE10 compared to that for AZ31 corresponds to the formation of higher ears in the ZE10 cups. Furthermore, earing valleys in the RD and TD are expected in the case of a negative Δr value [19] and this also corresponds to the earing behaviour of the ZE10 cups in the present study.

Fig. 7 presents the thickness strain measured at different positions of the successfully drawn cups. Measuring position 1 corresponds to the mid-point of the bottom plate, pos. 3 ~ pos. 5 to the curvature, pos. 6 to the necking region near to the punch radius and pos. 7 to the mid-height of the wall, as illustrated in Fig. 7 (b). The strain values given in Fig. 7 (a) were calculated by assuming that the thickness at the mid-point of the bottom plate is the same as that of the initial sheet. The amount of thickness reduction in the ZE10 cups is in general high at all forming temperatures, while the thickness strains of the AZ31 cups depend on the

forming temperature. The AZ31 cups drawn at 200 °C and 250 °C have smaller thickness reductions at the curvature and larger thickening at the wall than the ZE10 cups drawn at the same temperatures. The AZ31 cup drawn at 300 °C, however, shows thickness strains similar to that of the ZE10 cups. The greater reduction in thickness of the ZE10 cups corresponds to the characteristic texture of the initial sheet as described above, where the thickness strain can be accommodated easily by basal <a> slip. The dependency of the thickness strain of the AZ31 cups on the forming temperature indicates that the main deformation modes and the deformation behaviour change with the temperature. The AZ31 cups can be formed successfully at working temperatures above 200 °C. This temperature is high enough for dynamic recrystallisation (DRX) as well as for the activation of deformation modes which are hard to activate at room temperature [33, 34]. Furthermore, the role of the working temperature can not be considered in terms of the r values measured at room temperature, although there is general agreement between the earing behaviour and the measures of the planar anisotropy of the AZ31 and ZE10 sheets. The effect of the working temperature and associated microstructural changes on the deep drawing behaviour will be discussed in the following section based on EBSD results.

3.3. Microstructure of deep drawn AZ31 cups

Fig. 8 displays EBSD boundary maps at the wall of the AZ31 cups drawn at different temperatures. High angle boundaries (>15°) are marked in black. Twin boundaries are marked with different colours depending on their types, which are identified by their misorientation relations expressed as axis-angle pairs: $\{10\bar{1}2\}$-tensile twin (<$11\bar{2}0$>, 86°, red), $\{10\bar{1}1\}$-compression twin (<$11\bar{2}0$>, 56°, yellow) and $\{10\bar{1}1\}$-$\{10\bar{1}2\}$secondary twin (<$11\bar{2}0$>, 38°, greeen) [35]. The related textures using EBSD data measured at the walls are shown as re-calculated (0001) and $\{10\bar{1}0\}$ pole figures in Fig. 9. They are rotated in such way that they have the same sample coordinate system as that of the initial sheets in Fig. 2. The bottom

regions of the drawn cups experienced almost negligible deformation during deep drawing. Moreover, they were kept near room temperature, because of the direct contact with the unheated punch, while the wall parts were kept at the drawing temperature. The microstructure and texture at the bottom, therefore, are similar to those of the initial rolled sheets. For these reasons, the microstructures developed at the wall are considered in the present study.

The AZ31 cup drawn at 150 °C, which fractured during deep drawing, shows a large amount of tensile twins, whereas the cup drawn at 200 °C has fewer tensile twins, Fig. 8 (a) and (b). The texture component corresponding to the tensile twinning is visible in the pole figures and marked as dashed circles in Fig. 9 (a) and (b). The areas with the texture component corresponding to tensile twinning are marked with the colour blue in the EBSD boundary maps, Fig. 8. Considering the texture of the AZ31 sheet and the strain conditions during deep drawing, the observed tensile twins are mainly caused by compressive strains along the blank circumferential direction at the flange. For the activation of tensile twins, a tensile strain along the crystallographic c-axes of the matrix grain is required. Most grains of the AZ31 sheet have their c-axes in the sheet thickness direction. Hence, the compressive stress along the blank circumferential direction, which causes the thickening of the blank, provides tensile strain in the thickness direction. Since the strain which can be accommodated by tensile twinning is limited (e.g. $\varepsilon = 0.065$ can be accommodated even in the case of full tensile twinning) the activation of further deformation systems has to be considered in order to explain the successful deep drawing of the AZ31 cup at 200 °C. In this cup, large internal misorientations within a grain and many low angle boundaries in the vicinity of the matrix grain boundaries are visible. As marked with arrows in Fig. 8 (d), the formation of small grains with high angle boundaries is observed in the mantle of the matrix grains. This experimental observation implies DRX by a dynamic rotation mechanism as suggested by Ion et al. [33]. Furthermore, the occurrence of DRX indicates that non-basal slip systems are activated during deformation,

because the formation of high angle boundaries is promoted by non-basal slip. Since basal <a> slip causes a lattice distortion mainly around the basal planes of the matrix grains, this is not enough for the formation of new boundaries. In order to build a new boundary a continuous arrangement of dislocations is required, i.e. dislocations on the basal planes as well as on non-basal planes. This can be achieved by the activation of non-basal slip and / or cross slip of the basal dislocations onto non-basal planes [34].

The AZ31 cups show the development of a (0001)<10$\bar{1}$0> texture component, where the crystal plane (0001) is oriented perpendicular to the thickness direction and the crystal direction <10$\bar{1}$0> is oriented parallel to the deep drawing direction, specifically after forming at 200 °C, Fig. 9 (b). The formation of this texture corresponds to a rotation around the c-axes of the initial texture and cannot be explained by basal <a> slip alone. The basal <a> slip system generally causes a crystal rotation in such way that the basal planes align parallel to the tensile axes, e.g. as a <10$\bar{1}$0> fibre texture component parallel to the tensile axes. Koike et al [36] reported, from TEM and slip line trace studies that prismatic <a> slip leads to the formation of such a (0001)<10$\bar{1}$0> texture component during the tensile loading of a rolled AZ61 sheet. Moreover, the critical resolved shear stresses (CRSS) for non-basal slip systems decrease with increasing temperature [33, 37]. Thus, the development of the (0001) <10$\bar{1}$0> texture component and the occurrence of DRX in the deep-drawn cups of AZ31 can be understood by the activation of prismatic <a> slip.

The AZ31 cup drawn at 300 °C shows a different microstructure compared to those drawn at lower temperatures. Tensile twins are no longer observed. Conglomerates of fine, dynamically recrystallised grains are seen to be aligned along directions rotated about 30° from the drawing direction, as indicated by the dashed lines in Fig. 8 (c). Accordingly, the texture component related to tensile twinning is absent, Fig. 9 (c). The fine grains surrounding the large grains are characteristic for Mg alloys after sufficient progress of DRX. The fine grains aligned within the bands are developed in the vicinity of the boundaries of the large

matrix grains by a dynamic rotation mechanism. Further deformation is concentrated in these fine grains at the mantle of the matrix grains, such that DRX within these areas is promoted. Subsequently, band-shaped conglomerates of fine grains are developed, in which a large amount of the deformation can be accommodated by dislocation slip [38]. Thus, the formability of the AZ31 sheet increases due to the occurrence of DRX. Moreover, the cups drawn at 300 °C show a large thickness strain similar to that of the ZE10 cups, Fig. 7. The texture of the drawn cup at this high temperature, Fig. 9 (c), corresponds to the preferred alignment of the crystal c-axes parallel to the thickness direction, which is similar to that of the initial sheet, Fig. 2 (b). Thus, the large thickness strain cannot be accommodated by <a> dislocation slip. A deformation mechanism accompanying the strain along the c-axes is required for accommodating strain along the thickness direction, especially for the large negative strain at the necking area which cannot be explained by tensile twinning in this specific case. Deformation mechanisms that accommodate a contraction along the c-axes are compression twinning and <c+a> pyramidal slip. However, compression twins are not observed in these AZ31 cups. Thus, the large thickness strain in the AZ31 cups drawn at 300 °C can be explained by <c+a> slip.

Assuming that the degree of DRX is dependent on the amount of non-basal slip activated, the deformation accommodated by non-basal slip and especially by <c+a> slip is higher at 300 °C than at 200 °C. In fact, the thickness reduction of the former cup is much larger than the latter cup, Fig. 7. The thickness reduction observed in the AZ31-200 °C cup indicates that <c+a> slip contributes to the deformation at 200 °C, however, in a small amount. In addition, DRX should also play an important role in accommodating thickness strain, because the dynamically recrystallised grains have different orientations to the matrix. Then, the thickness strain can also be accommodated by basal <a> slip in the case that the c-axes of the recrystallised grains are tilted from the sheet thickness direction. The relationship between the activity of non-basal slip, the degree of DRX and the amount of thickness strain at the

different temperatures is consistent with results in the literature showing that the r-value of the AZ31 alloy decreases with increasing temperature. The recently published study of Nebebe et al [21] clearly shows the decrease of the r-values at 200 °C, especially in the AZ31 alloy. The r-values measured at 200 °C of the ZE10 alloy does show only slight difference comparing to those at room temperature (AZ31: $\bar{r}$ =1.53 and $2\Delta r/\bar{r}$ = 0.07, ZE10: $\bar{r}$ =1.24 and $2\Delta r/\bar{r}$ =-0.36, measured at 200°C and at strain rate of 0.02/sec, calculated from the results in the above literature.). Though the r-values at high temperature are influenced by the activation of additional deformation mechanisms and the occurrence of the DRX, the r-values measured at room temperature surprisingly show a similar tendency with that measured at 200 °C, particularly in the normalised r-values.

3.4. Microstructure of deep drawn ZE10 cups

The EBSD boundary maps and the textures measured at the walls of the ZE10 cups are presented in Figs. 10 and 11, respectively. The microstructural features are significantly different to those of AZ31. At 150 °C, the microstructure contains not only tensile twins but also compression and secondary twins, Fig. 10 (a). The twinned area decreases with increasing drawing temperature, such that at 300 °C only few twins are found. Moreover, the ZE10 cups do not show DRX, even at 300 °C, but the grains are stretched in the deep drawing direction. The texture of the ZE10 cups is characterised as a <10$\bar{1}$0> fibre component parallel to the drawing direction, Fig. 11. As discussed above, the development of such a <10$\bar{1}$0> fibre texture is caused mainly by basal <a> slip. At 200 °C and 300 °C the basal poles are distributed continuously from the cup thickness to the circumferential direction, whereas at 150 °C the basal poles are located mainly in the circumferential direction. The high concentration of basal poles in the circumferential direction in the cup drawn at 150 °C is likely to be a result of a large amount of twinning. The orientation changes due to secondary and tensile twinning are presented in the stereographic projection of the basal poles, Fig. 12.

The orientation change generated by tensile twinning is the same as that found in the AZ31 cups, i.e. about 90° rotation of the basal pole from the cup thickness direction into the cup circumferential direction, Fig. 12 (b). Secondary twinning occurs mainly in the matrix grains having c-axes largely tilted from the thickness direction. As shown in Fig. 12 (c), the secondary twinned areas also have c-axes tilted far from the thickness direction. Consequently, the basal poles of the cup drawn at 150°C are mainly located near to the cup circumferential direction. It is worthwhile to notice that the twinning types observed at 150°C show a strong dependence on the orientation of the matrix grains. In the case of grain 'A' in Fig. 12 (a), which shows a secondary twin, the c-axis is parallel to the cup circumferential direction, which is subjected to a compressive stress. The c-axes of the grains 'B' and 'C' are inclined by about 30° to the compression direction (the cup circumferential direction). Interestingly, the c-axes of the grains containing compression and/or secondary twins lie along the thickness – circumferential direction, i.e. the equator of the (0001) pole figure. This indicates that the compressive strain during deep drawing of the ZE10 cup at 150 °C is accommodated by compression and secondary twinning. Tensile twins in the grains ('D' and 'E') have their c-axes parallel to the thickness direction and can be explained in a similar way to those in the AZ31 cups, Fig. 8 and 9.

In the cups drawn at 200 °C and 300 °C a continuous distribution of basal poles is observed. The amount of twinning decreases with increasing drawing temperature and is very small at 300 °C. Barnett et al [39] have reported that the activity of twinning decreases with increasing deformation temperature. They have shown that the change from twinning dominated to slip dominated deformation occurs at a transition temperature which coincides with that for the activation of non-basal slip. Although the extent of non-basal slip increases with increasing temperature, the deformation caused by deep drawing of the ZE10 cups is accommodated mostly by basal <a> slip since the initial texture is favourable for this deformation system. Moreover, the microstructural features of the ZE10 cups, e.g. retardation of DRX and

development of the <10$\bar{1}$0> fibre texture, corresponds to the high activity of basal <a> slip. Since basal <a> slip is activated more easily in ZE10 than in AZ31, deep drawing of ZE10 can be carried out successfully at lower forming temperatures.

Summary

The present study has demonstrated the influence of the initial texture on the mechanical response, anisotropy and the formability of AZ31 and ZE10 sheets, using tensile tests and round cup drawing. The AZ31 sheet has a strong basal-type texture with basal poles slightly inclined towards the rolling direction (RD). The ZE10 sheet has an oval-shaped distribution of basal poles at angles of about 40° to the sheet normal direction (ND). The distinct textures of the sheets result in significant differences in the deformation behaviour as well as microstructural evolution. The main results of the study are summarised as follows:

1. The AZ31 sheet shows high r values (1.9 in the RD ~ 2.9 in the TD), which are mainly caused by the basal-type texture and the following difficulties of the thickness straining. The r values increase gradually from RD to TD of the AZ31 sheet. The ZE10 sheet shows low r values as a result of the favourable texture for basal <a> slip. The r value in the direction 45° to the RD is higher than that in the RD and the TD (0.9 in the RD, 0.8 in the TD and 1.2 in the 45° direction).

2. The minimum temperature for the successful deep drawing is 150 °C for the ZE10 sheet and 200 °C for the AZ31 sheet. Despite the high normal anisotropy values the deep drawn AZ31 cups show negligible earing, while the ZE10 cups show considerable earing phenomena. The earing behaviour of drawn cups of both alloys can be correlated with the measured r values by employing the normalised planar anisotropy ($2\Delta r/\bar{r}$ = 0.27 for AZ31, -0.64 for ZE10 sheet).

3. At the wall of the successfully drawn AZ31 cups, the occurrence of DRX and the formation of an (0001) $<10\bar{1}0>$ texture component were observed. The development of the (0001) $<10\bar{1}0>$ texture component at 200 °C is mainly a result of extensive prismatic <a> slip. With increasing forming temperature, the volume fraction of DRXed grains becomes larger and the intensity of the (0001) $<10\bar{1}0>$ texture component decreases. This indicates the activation of other deformation mechanisms, e.g. <c+a> slip and localised deformation in the DRXed grains. The magnitude of the thickness strain ε_T increases with forming temperature and at 300 °C reaches a value similar to that of the ZE10 cups.

4. The ZE10 cup drawn at 150 °C shows extensive compression and secondary twinning by which the contraction along the c-axes can be accommodated. Moreover, the compression and secondary twins are observed in matrix grains having c-axes tilted towards the cup circumferential direction, subjected to compressive stresses during deep drawing. With increasing forming temperature, the extent of twinning decreases and the $<10\bar{1}0>$ fibre texture parallel to the drawing direction becomes clearer. Because thickness strains can be accommodated easily in the ZE10 sheet by compression and secondary twinning and also by dislocation slip including basal <a> slip, the ZE10 cups show large ε_T values independent of the forming temperature.

Acknowledgements

The authors are grateful to Dr. P. Beaven for fruitful discussion and to V. Kree in GKSS Research Centre for technical supports. It is gratefully acknowledged the financial support of German Research Foundation DFG (under grant LE 1395/3-1).

References

[1] Kocks UF, Tomé CN, Wenk HR. Texture and Anisotropy. Cambridge: Cambridge University Press; 1998.

[2] Philippe MJ. Mater Sci Forum 1994;157-162;1337

[3] Pérez-Prado MT, Del Valle JA, Contreras JM, Runao OA. Scripta Mater 2004; 50; 661

[4] Styczynski A, Hartig Ch, Bohlen J, Letzig D. Scripta Mater 2004; 50; 943

[5] Yoo MH, Morris JR, Ho KM, Agnew SR. Metall Mater Trans 2000; 33A; 813

[6] Watanabe H, Mukai T, Ishikawa K. J Mater Processing Tech 2007; 182; 644

[7] Huang X, Suzuki K, Watazu A, Shigematsu I, Saito N. Mater Sci Eng 2008; A488; 214

[8] Kim WJ, Lee JB, Kim WY, Jeong HT, Jeong HG. Scripta Mater 2007; 56; 309

[9] Bohlen J, Nürnberg MR, Senn JW, Letzig D, Agnew SR. Acta Mater 2007; 55; 2101

[10] Stanford N, Barnett M. Scripta Mater 2008; 58; 179

[11] Chino Y, Kado M, Mabuchi M. Mater Sci Eng 2008; A494; 343

[12] Chino Y, Sassa K, Mabuchi M. Mater Sci Eng 2009; A513-514; 394

[13] Mishra RK, Gupta AK, Rao PR, Sachdev AK, Kumar AM, Luo AA. Scripta Mater 2008; 59; 562

[14] Doege E, Dröder K. J Mater Processing Tech 2001; 115; 14

[15] Palumbo G, Sorgente D, Tricarico L, Zhang SH, Zheng WT. J Mater Processing Tech 2007; 191; 342

[16] Yang LF, Mori KI, Tsuji H. Trans Nonferrous Met Soc China 2008; 18; 86

[17] Zhang SH, Zhang K, Xu YC, Wang ZT, Xu Y, Wang ZG. J Mater Processing Tech 2007; 185; 147

[18] Lee YS, Kim MC, Kim SW, Kwon YN, Choi SW, Lee JH. J Mater Processing Tech 2007; 187-188; 103

[19] Hosford WF, Caddell RM. Metal Forming: Mechanics and Metallurgy. Cambridge; Cambridge University Press; 2007

[20] Ghosh AK, Hecker SS, Keeler SP. In: Dieter GE, editor. Workability Testing Techniques.; ASM Intl; 1984

[21] Nebebe M, Bohlen J, Steglich D, Letzig D. In: Proc. 12th International ESAFORM Conference on Material Forming: In Press.

[22] Agnew SR, Yoo MH, Tomé CN. Acta Mater 2001; 49; 4277

[23] Agnew SR, Duygulu Ö. Int J Plasticity 2005; 21; 1161

[24] Kaiser F, Bohlen J, Letzig D, Styczynski A, Hartig Ch, Kainer KU. Mater Sci Forum 2003; 419-422; 315

[25] Wonsiewicz BC, Backofen WA. Trans Metall Soc AIME 1966; 239; 1422

[26] Yi SB, Schestakow I, Zaefferer S. Mater Sci Eng A 2009; 516; 58

[27] Mackenzie LWF, Pekguleryuz MO. Scripta Mater 2008; 59; 665

[28] Ball EA, Prangnell PB. Scripta Metal Mater 1994; 31; 111

[29] Stanford N, Barnett MR. Mater Sci Eng 2008; A469; 399

[30] Wendt J, Kainer KU, Arruebarrena G, Hantzsche K, Bohlen J, Letzig D. In: Nyberg A, Agnew SR, Neelameggham R, Pekguleryuz O, editor. Magnesium Technology 2009 San Francisco; TMS; 2009

[31] Lee DN. J Mater Sci Letters 1984; 3; 677

[32] Wilson DV, Butler RD. J Institute Metals 1962; 90; 473

[33] Ion SE, Humpreys FJ, White SH. Acta Metall 1982; 30; 1909

[34] Galiyev A, Kaibyshev R, Gottstein G. Acta Mater 2001; 49; 1199

[35] Al-Samman T, Gottstein G. Mater Sci Eng 2008; A488; 406

[36] Koike J, Ohyama R. Acta Mater 2005; 53; 1963

[37] Patridge PG. Metall Review 1967; 12; 169

[38] Del Valle JA, Pérez-Prado MT, Ruano OA. Mater Sci Eng 2003; A355; 68

[39] Barnett MR, Keshavarz Z, Beer AG, Atwell D. Acta Mater 2004; 52; 5093

List of Tables

List of Figures

Fig. 1 Microstructures of (a) AZ31 and (b) ZE10 sheets. (c) Grain size distributions in both alloys. The colour code of the EBSD maps corresponds to the inverse pole figure in the ND.

Fig. 2 Recalculated (0001) and $\{10\bar{1}0\}$ pole figures of the as-received (a) AZ31 and (b) ZE10 sheets (contour levels = 1, 1.5, 2, 2.5, 3, 4, 5,… , 13 multiple random degree). Density profiles of the basal pole along different sheet directions are shown for (c) AZ31 and (d) ZE10 sheets, (RD: rolling direction, TD: transverse direction, 45°: 45° from the RD).

Fig. 3 Stress-strain curves of the (a) AZ31 and (b) ZE10 sheets in different tensile loading directions.

Fig. 4 Width strain, ε_w, of the (a) AZ31 and (b) ZE10 sheets as a function of the tensile elongation, ε_l, during tensile loading in different sheet directions.

Fig. 5 Deep drawn cups formed at different temperatures; (a) failed and (b) successfully drawn cups. White arrows indicate the rolling direction of the sheets.

Fig. 6 Variation of the earing heights, Z, at different deep drawing temperatures.

Fig. 7 (a) Thickness strains of the AZ31 (filled symbols) and ZE10 (opened symbols) cups drawn at different temperatures. (b) The positions of the thickness measurements (the necking and the thickening at the wall is exaggeratingly illustrated).

Fig. 8 EBSD boundary maps at the wall thickness plane of the AZ31 cups drawn at different temperatures; (a) 150 °C, (b) 200 °C, (c) 300 °C. (d) EBSD inverse pole figure map of the

AZ31 cup drawn at 200 °C. Arrows indicate the formation of large angle boundaries in the vicinity of the matrix grain boundaries.

Fig. 9 (0001) and $\{10\bar{1}0\}$ pole figures calculated using the EBSD data from AZ31 cups drawn at different temperatures: (a) 150 °C, (b) 200 °C, (c) 300 °C (contour levels = 1, 2, … , 13 multiple random degree). The strain states and sample coordinates during deep drawing are shown in (d). The position of the EBSD measurement is also marked.

Fig. 10 EBSD boundary maps of the ZE10 cups drawn at different temperatures; (a) 150 °C, (b) 200 °C, (c) 300 °C.

Fig. 11 (0001) and $\{10\bar{1}0\}$ pole figures calculated using the EBSD data from ZE10 cups drawn at different temperatures: (a) 150 °C, (b) 200 °C, (c) 300 °C (contour levels = 1, 2, … , 5 multiple random degree).

Fig. 12 (a) EBSD boundary map of the ZE10 cup drawn at 150 °C. Stereographic projection of the basal poles showing the orientation changes generated by secondary twinning and tensile twinning, (b) and (c) respectively. The orientation of the matrix grains is coloured as black / grey, the secondary twinned area as green and the tensile twinned area as red / orange.

	Tensile direction	YS (MPa)	UTS (MPa)	Elong. (%)	r_8
AZ31	RD	163	263	16	1.92
	45°	175	263	19	2.11
	TD	186	275	17	2.92
ZE10	RD	143	228	16	0.93
	45°	120	221	22	1.23
	TD	110	220	18	0.85

Tab. 1

	Deep drawing temperature (°C), $\beta = 1.7$				
	100	150	200	250	300
AZ31	F	F	G	G	G
ZE10	F	G	G	G	G

Tab. 2

	$\bar{r}$ (RT)	Δr (RT)	$2\Delta r/\bar{r}$ (RT)
AZ31	2.27	0.3	0.27
ZE10	1.06	-0.34	-0.64

Tab. 3

(a)

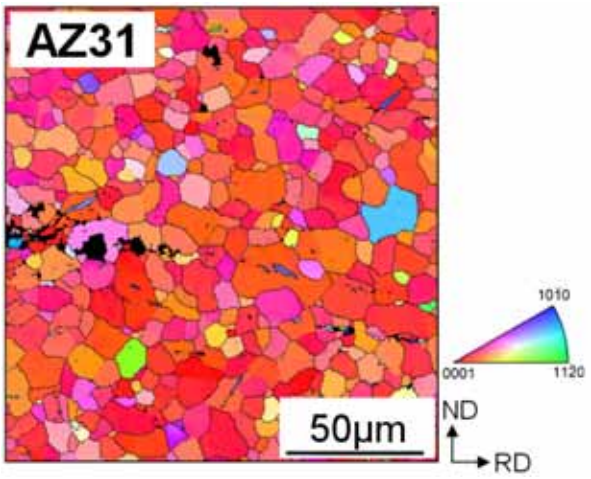
AZ31
50μm
1010
0001
1120
ND
RD

(b)

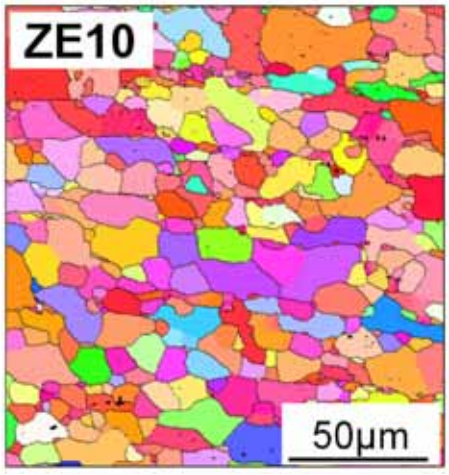
ZE10
50μm

(c)

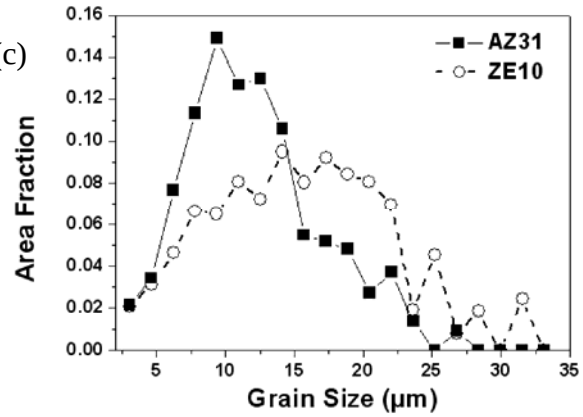
AZ31
ZE10
Area Fraction
Grain Size (μm)
0.00
0.02
0.04
0.06
0.08
0.10
0.12
0.14
0.16
5
10
15
20
25
30
35

Fig.1

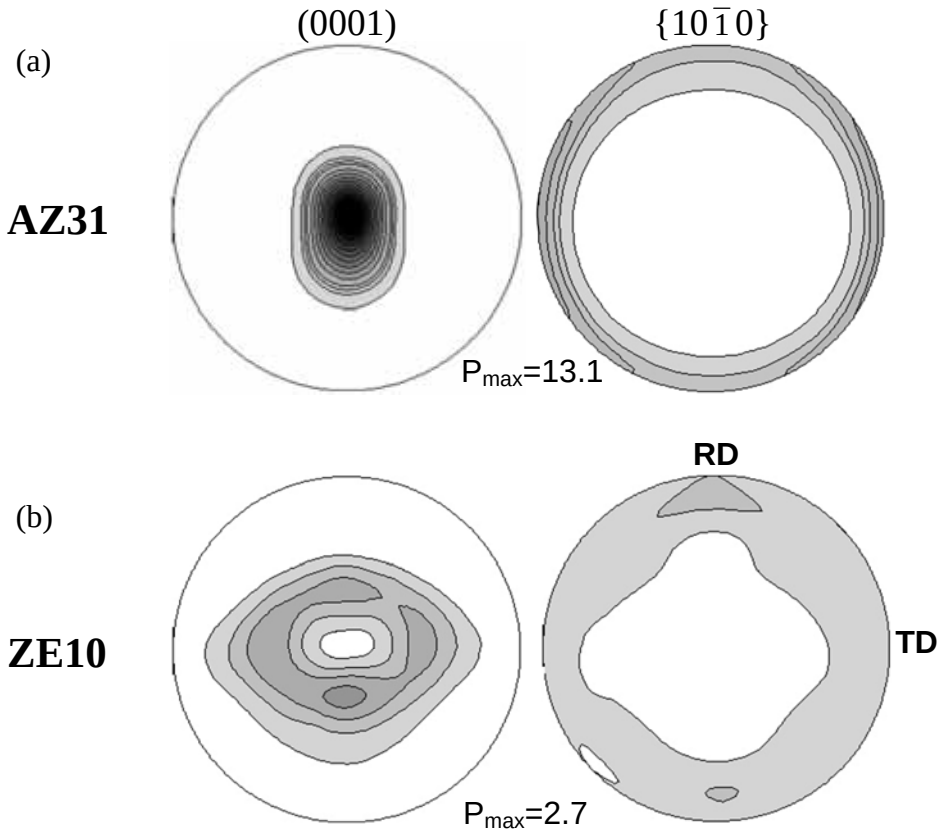
(a)
(0001)
{10$\bar{1}$0}
AZ31
P_{max}=13.1
(b)
RD
ZE10
TD
P_{max}=2.7

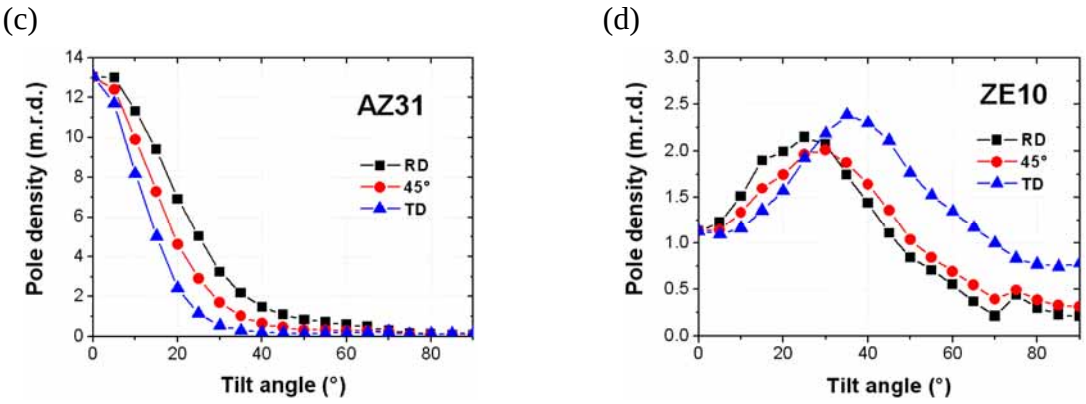
(c)
AZ31
RD
45°
TD
Pole density (m.r.d.)
Tilt angle (°)
(d)
ZE10
RD
45°
TD
Pole density (m.r.d.)
Tilt angle (°)

Fig. 2

(a)

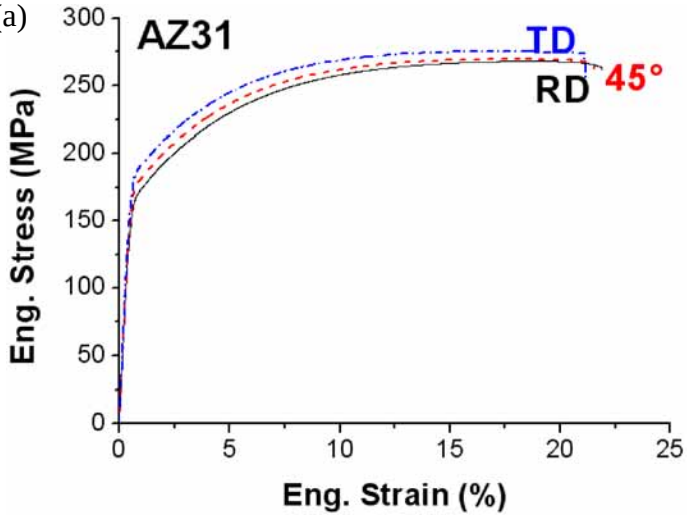
AZ31
TD
RD
45°
Eng. Stress (MPa)
Eng. Strain (%)
0
50
100
150
200
250
300
0
5
10
15
20
25

(b)

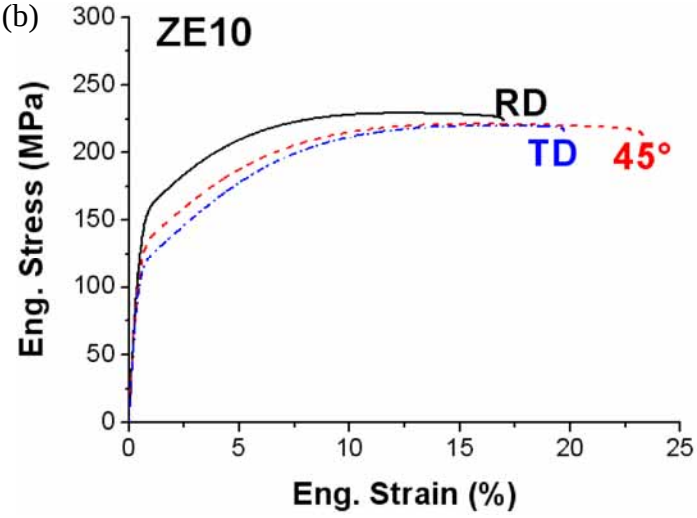
ZE10
RD
TD
45°
Eng. Stress (MPa)
Eng. Strain (%)
0
50
100
150
200
250
300
0
5
10
15
20
25

Fig. 3

(a)

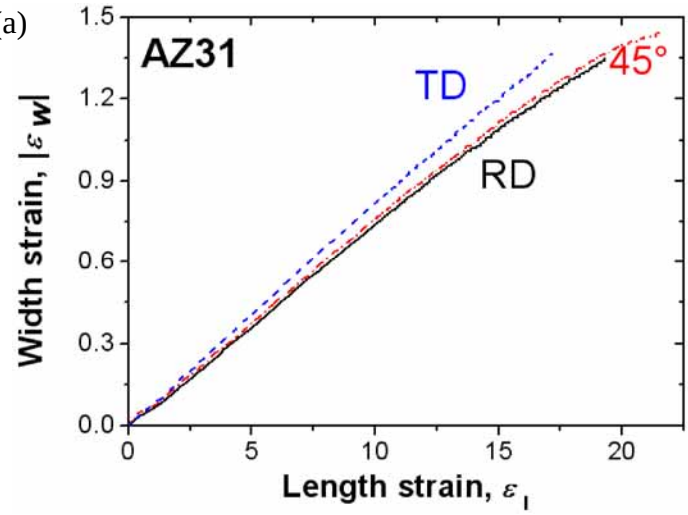
AZ31
TD
45°
RD
Width strain, |ε w|
Length strain, ε l
0.0
0.3
0.6
0.9
1.2
1.5
0
5
10
15
20

(b)

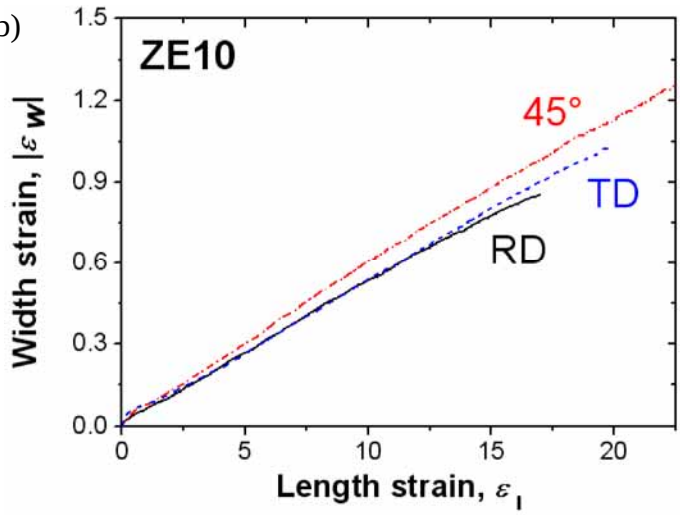
ZE10
45°
TD
RD
Width strain, |ε w|
Length strain, ε l
0.0
0.3
0.6
0.9
1.2
1.5
0
5
10
15
20

Fig. 4

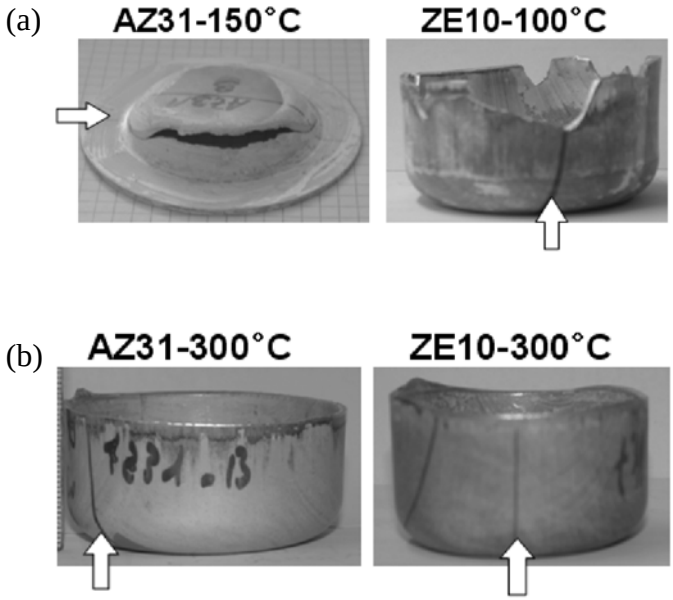

Fig. 5

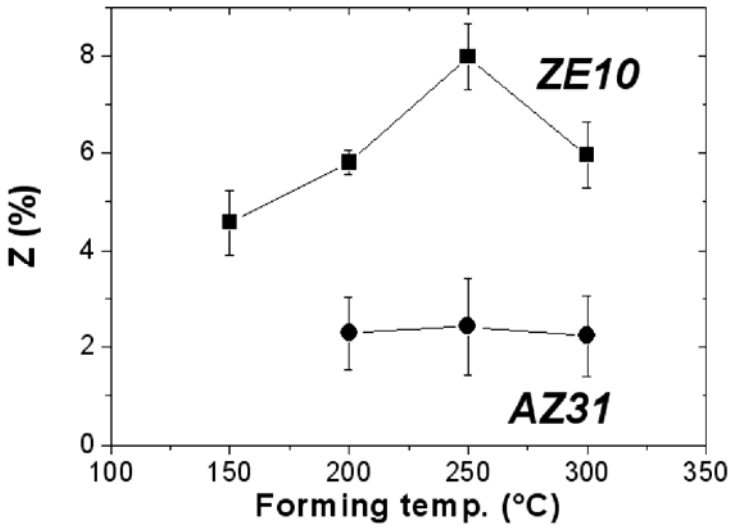

Fig. 6

(a)

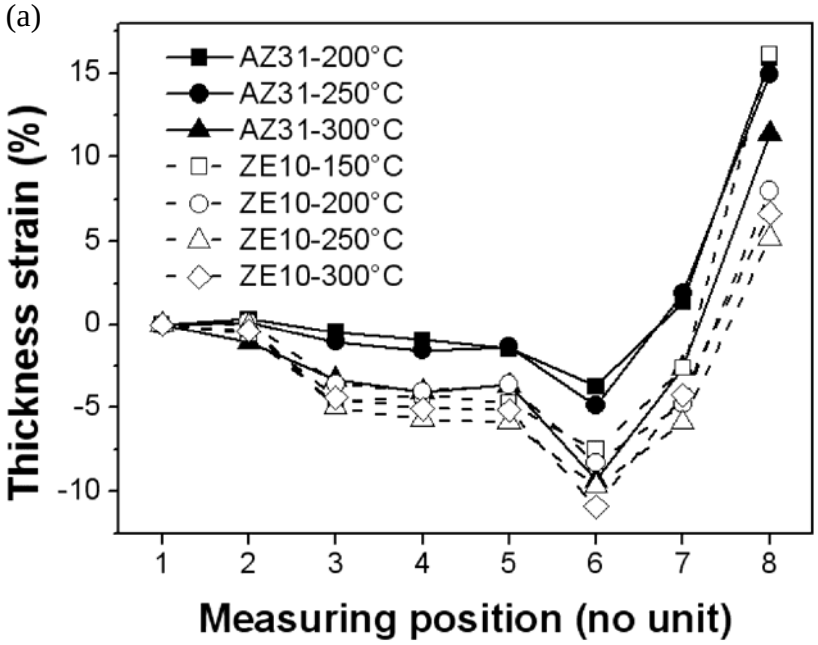
AZ31-200°C
AZ31-250°C
AZ31-300°C
ZE10-150°C
ZE10-200°C
ZE10-250°C
ZE10-300°C
Thickness strain (%)
15
10
5
0
-5
-10
1
2
3
4
5
6
7
8
Measuring position (no unit)

(b)

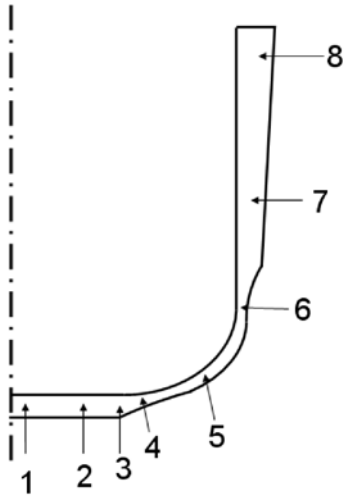
8
7
6
5
4
3
2
1

Fig. 7

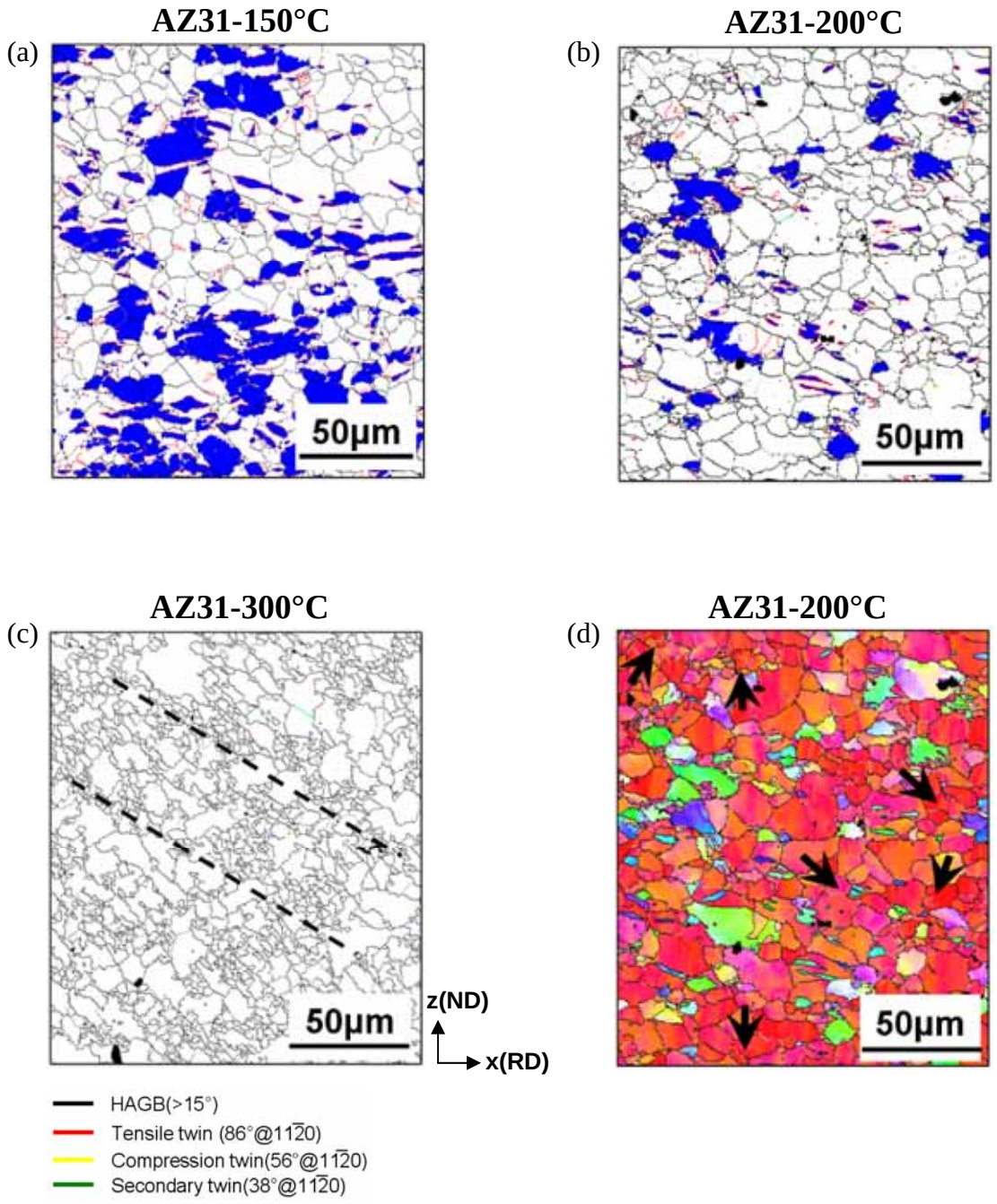
AZ31-150°C
(a)
50μm
AZ31-200°C
(b)
50μm
AZ31-300°C
(c)
50μm
z(ND)
x(RD)
AZ31-200°C
(d)
50μm
HAGB(>15°)
Tensile twin (86°@11$\bar{2}$0)
Compression twin(56°@1$\bar{1}$20)
Secondary twin(38°@11$\bar{2}$0)

Fig. 8

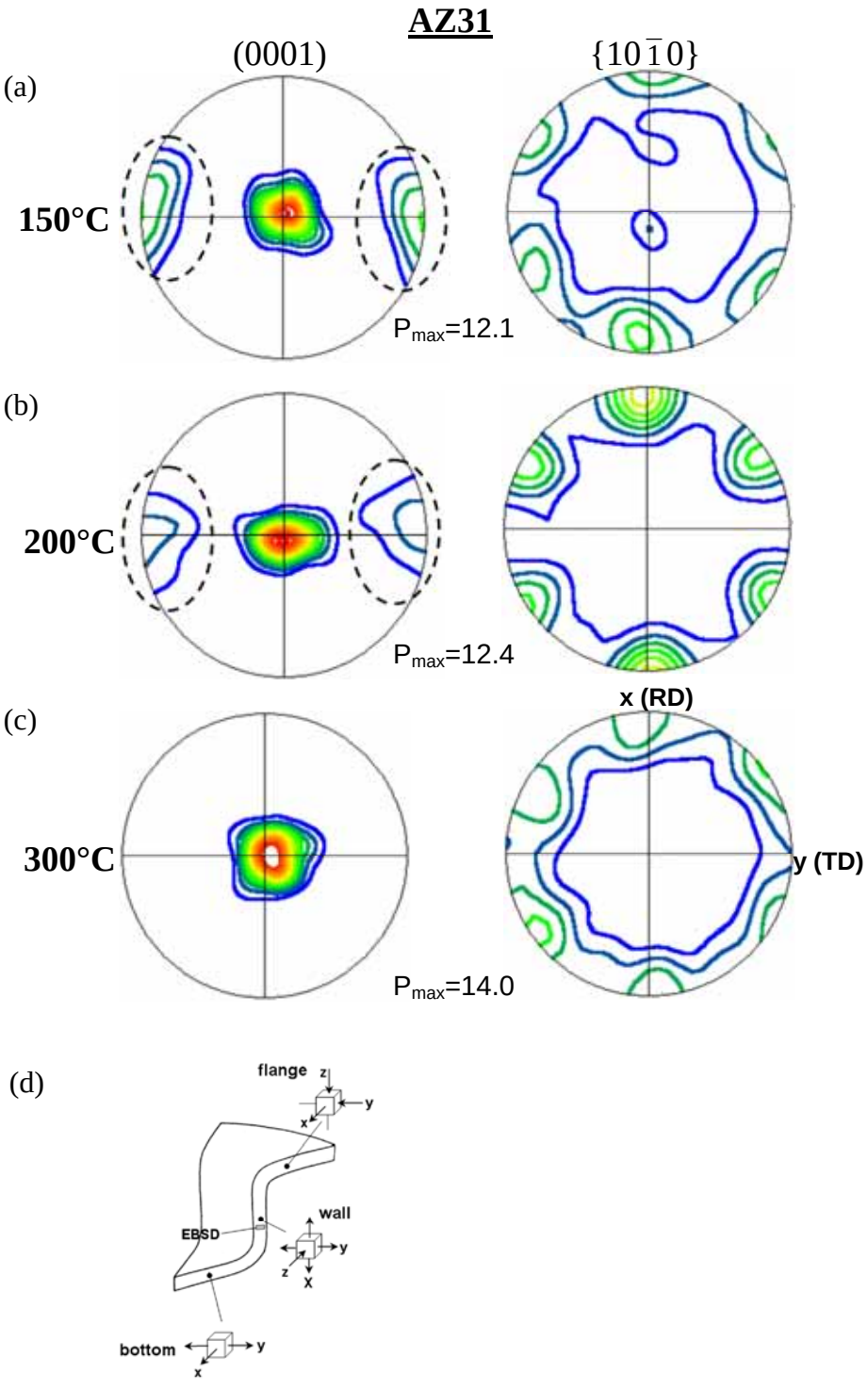
AZ31
(0001)
{10$\bar{1}$0}
(a)
150°C
P_{max}=12.1
(b)
200°C
P_{max}=12.4
x (RD)
(c)
300°C
y (TD)
P_{max}=14.0
(d)
flange
z
y
x
wall
EBSD
y
z
X
bottom
y
x

Fig. 9

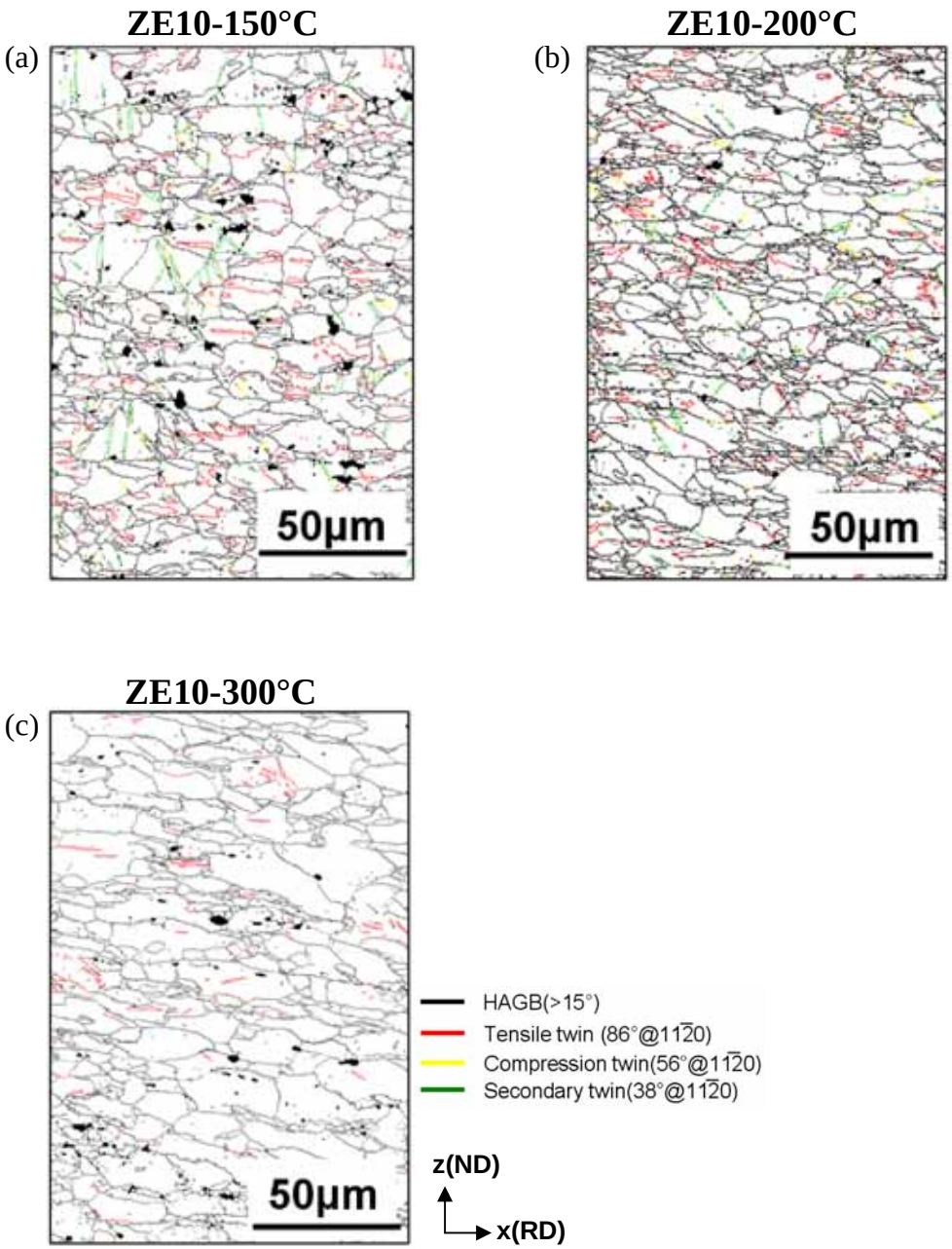
ZE10-150°C
(a)
50μm
ZE10-200°C
(b)
50μm
ZE10-300°C
(c)
50μm
HAGB(>15°)
Tensile twin (86°@11$\bar{2}$0)
Compression twin(56°@11$\bar{2}$0)
Secondary twin(38°@11$\bar{2}$0)
z(ND)
x(RD)

Fig. 10

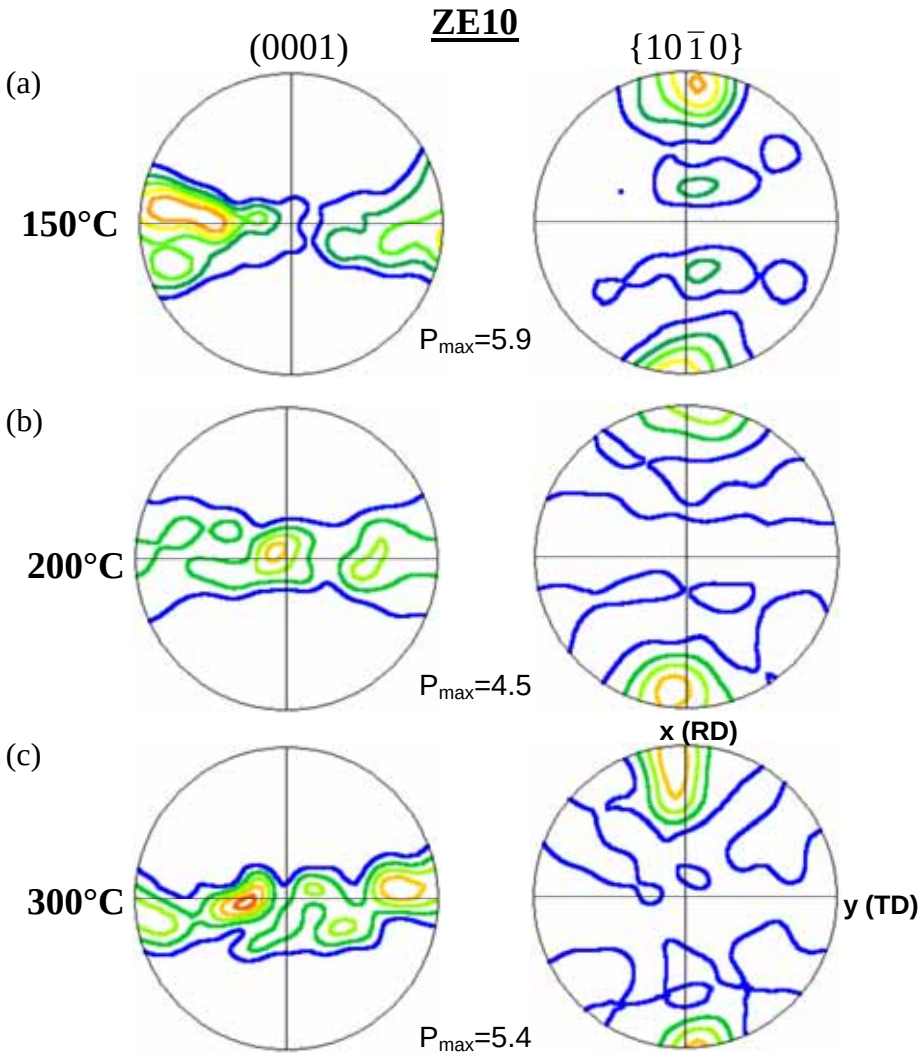
ZE10
(0001)
{10$\bar{1}$0}
(a)
150°C
P_{max}=5.9
(b)
200°C
P_{max}=4.5
x (RD)
(c)
300°C
y (TD)
P_{max}=5.4

Fig. 11

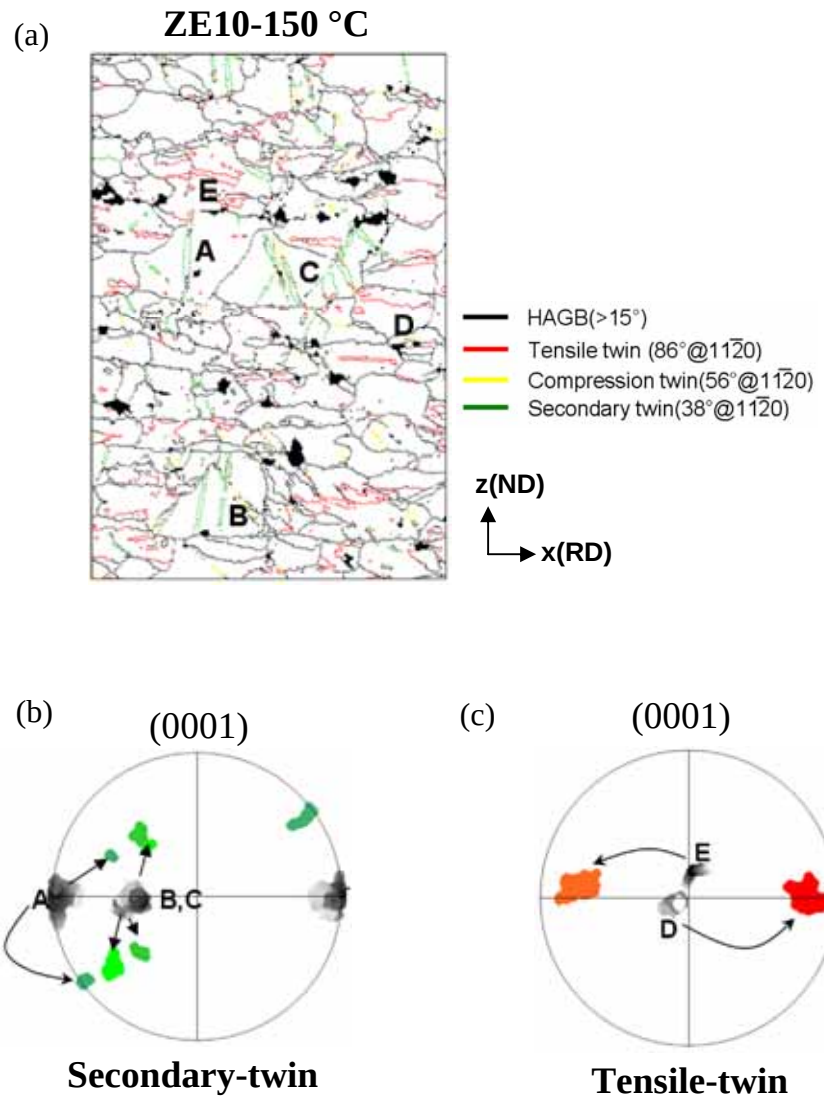
(a)
ZE10-150 °C
E
A
C
D
B
HAGB(>15°)
Tensile twin (86°@11$\bar{2}$0)
Compression twin(56°@1$\bar{1}$20)
Secondary twin(38°@11$\bar{2}$0)
z(ND)
x(RD)
(b)
(0001)
A
B,C
Secondary-twin
(c)
(0001)
E
D
Tensile-twin

Fig. 12